ChemComm

# High Performance Sodium-Sulfur Battery at Low Temperature Enabled by Superior Molten Na Wettability



| | |
|---|---|
| Journal: | *ChemComm* |
| Manuscript ID | CC-COM-10-2020-006987.R1 |
| Article Type: | Communication |
| | |

COMMUNICATION

# High Performance Sodium-Sulfur Battery at Low Temperature Enabled by Superior Molten Na Wettability

Received 00th January 20xx,
Accepted 00th January 20xx

DOI: 10.1039/x0xx00000x

Minyuan M. Li[a], Xiaochuan Lu[b,*], Xiaowen Zhan[c], Mark H. Engelhard[a], Jeffrey F. Bonnett[a], Eugenia Polikapov[a], Keeyoung Jung[d], David M. Reed[a], Vincent L. Sprenkle[a], and Guosheng Li[a,*]

**Reducing the operating temperature of conventional molten sodium-sulfur batteries (~350 °C) is critical to create safe and cost-effective large-scale storage devices. By raising the surface treatment temperature of lead acetate trihydrate, sodium wettability on β"-$Al_2O_3$ improved signficantly at 120 °C. The low temperature Na-S cell can reach a capacity as high as 520.2mAh/g and stable cycling over 1000 cycles.**

The rise of renewable energy presses for the development of the next-generation large-scale electrochemical energy storage devices, targeting low materials cost/production cost, long operation lifetime, and robust safety/reliability standard.[1] While lithium-ion batteries remain one of the strongest candidates due to their high energy density, relatively expensive materials and limited lifetime, coupled with concerns for safety, call for further development of energy storage using cheap and abundant materials.[2] In those cases, sodium-based systems that offer comparable performance at a significantly reduced cost are much more promising.[3, 4]

Among different types of sodium-ion/metal batteries, the well-studied Na beta-alumina batteries (NBBs), with a β"-$Al_2O_3$ solid electrolyte (BASE) separating a molten sodium metal anode and a molten or semisolid cathode, have a strong technical foundation towards commercialization.[4, 5] Within conventional NBBs, different cathode materials establish two subgroups: sodium-metal halide and sodium-sulfur. Sodium-metal halide (Na-MH or ZEBRA) batteries use solid transition metal halides (e.g., $NiCl_2$ or $FeCl_2$) as the cathode material. They operate typically around 280 °C with a molten salt electrolyte, e.g. $NaAlCl_4$ (m.p. 157 °C), which is inert to the cathodic reactions and ensures rapid transport of sodium ions between the solid electrolyte and the solid cathode to achieve high activities.[6] On the other hand, sodium-sulfur (Na-S) batteries use molten sulfur/polysulfides as the cathode material and operate typically at 350 °C.[7] Although operating at higher temperatures, the state-of-art high-temperature Na-S batteries offer high system level energy and long-life expectancy (over 10 years) all at a low cost of materials.[8] In fact, conventional high-temperature molten Na-S batteries have already been in production and widely implemented as test units for grid storage or for supplementing wind and solar installations in Japan, Germany, the United Arab Emirates, and the United States of America.[9] While high-temperature molten Na-S batteries are indeed promising, the drawback to higher operating temperatures is that the cell components (sodium and polysulfides, etc.) are very active and can react violently if the BASE separator breaks.[10] The large exotherm along with evolving sulfur vapors, as seen in the recent incidents, profoundly demerit boarder commercialization and implementation of the high-temperature molten Na-S battery technologies.

Reducing the operating temperatures of molten Na-S batteries would retard the severity of discharge from cell failures and make them safer. Moreover, lower temperatures allow the integration of cost-effective polymer materials as seals, replacing more expensive techniques such as glass seal, thermo-compression bonding, and electron beam welding used for Na-S batteries in the past.[11, 12] We have previously demonstrated an intermediate-temperature (~150 °C) Na-S battery with an initial capacity of 473 mAh/g. The battery showed considerable capacity degradation during subsequent cycling (e.g., 30% for 60 cycles), which was attributed to the poor Na wettability on the surface of the BASE at lower temperatures.[13]

Improving sodium wetting by engineering the BASE-anode interface is one of the most important topics for low-temperature NBBs.[12, 14] Suppressing the formation of surface oxide films originated from surface adsorbates or impurities in

[a] *Electrochemical Materials and Systems Group, Pacific Northwest National Laboratory, Richland, WA 99352, USA*
[b] *Department of Applied Engineering Technology, North Carolina A&T State University, Greensboro, North Carolina 27411, USA Address here.*
[c] *College of Chemistry & Chemical Engineering, Anhui University, Hefei, Anhui 230601, P. R. China*
[d] *Materials Research Division, Research Institute of Industrial Science & Technology, Pohang, South Korea*

† Electronic Supplementary Information (ESI) available: experimental methods, specific capacity calculations, and scanning electron micrographs. See DOI: 10.1039/x0xx00000x

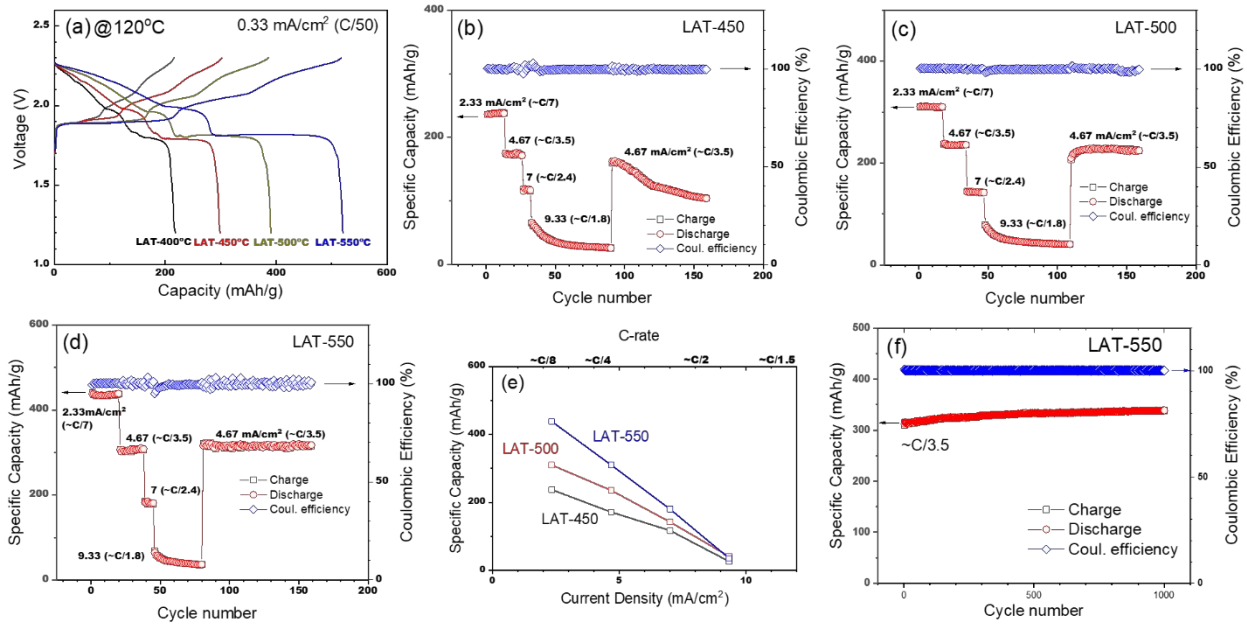


Figure 1. Battery performance of Na-S cells at 120 °C. (a) Voltage profiles of cells with BASE treated with lead acetate trihydrate (LAT) at various temperatures. (b—d) Capacity and coulombic efficiency for the Na-S cells with BASE treated with LAT at 450, 500, and 550 °C, respectively. (e) Specific capacity retention with respect to current density (C-rate). (f) Stable long-term cycling (C/3.5 and 1000 cycles) performance of Na-S cell with BASE treated with LAT at 550 °C.

the BASE can improve wettability.[15] Examples include coating the BASE surface with a thin layer of carbon, nickel, lead, bismuth, tin, lead/platinum; all can enhance the Na wetting to a certain extent.[16] On the other hand, adding other metals, such as cesium and potassium, to form alloyed sodium anodes also dramatically improve wettability.[17, 18] Both strategies were viable as demonstrated by our recent efforts on coating BASE with a thin layer of Pb particles and using Cs-Na alloys with excellent wetting performance at 200 °C and 150 °C respectively.[14, 17]

The surface modification method we studied by heat treating BASE with lead acetate trihydrate (LAT) between 210 and 400 °C is quite attractive, since this process is relatively simple and easy to scale up.[14] It was observed that the LAT treatment at 400 °C formed micron-size Pb spheres on BASE, where the corresponding Na wettability and battery performance were significantly better at 190°C. However, in contrast to the excellent Na wettability (low Na wetting angle at 16°) at near 200°C, much larger Na wetting angles (poor wetting), such as 146° and 108°, were observed at 150 °C and 175 °C, respectively, and this placed an obstacle for lowering the operating temperature beyond 150 °C.

In the current work, we further extend the heat treatment with LAT to higher temperatures. For the first time, excellent Na wetting is achieved at as low as 120 °C with the wetting angle almost reaching 0° (perfect Na wetting). To our knowledge, this work presents the best Na wetting performance on the surface of BASE using a simple and practical surface treatment method. The LAT treatment also allows Na-S cells to achieve a capacity as high as 520.2 mAh/g (C/50) at 120 °C and shows long-term cycling stability with the capacity and energy density at 338.5 mAh/g (~C/3.5) and 596.1 Wh/kg, respectively, over 1000 cycles. Meanwhile, the coulombic efficiency of the cell is greater than 99.99%, significantly higher than any typical room-temperature Na-S batteries with organic electrolytes. We here demonstrate a new, safer class of Na-S batteries that operates at significantly lower temperatures than the state-of-the-art high-temperature Na-S and ZEBRA batteries, while providing superior performance over room-temperature analogs.

We first noticed a significant improvement in battery performance when the surface treatment of BASE was performed at higher temperatures for identically prepared cells. At 120 °C, the voltage profiles of the cells (Figure 1a) with different LAT treatment temperatures show multiple steps during both the charge and the discharge stages. Similar to previous observations at 150 °C,[13] multistep reactions between Na and sulfur with the formation of various polysulfide species are likely happening.

With the LAT treatment for BASE at 400 °C, the initial cell (LAT-400) has a capacity at 120 °C is 216.1 mAh/g (Figure 1a), which is much lower than its theoretical capacity of 531.6 mAh/g (see Table 1S for more detailed capacity calculation). With LAT treatment at higher temperatures, the cell performance improves dramatically. As seen in Figure 1a, the cells have typical capacities of 301.9, 385.8, and 520.2 mAh/g (C/50) with the LAT treatment at 450 (LAT-450), 500 (LAT-500), and 550 °C (LAT-550), respectively. Considering the cell fabrication process is almost identical, the performance clearly depends on the BASE treatment condition, where the only variable is temperature. Previously, the cell with the LAT treatment at 400 °C had a typical capacity of 473 mAh/g (~C/50) operating at 150 °C.[13] The current LAT-550 cell has the initial capacity of 520.2 mAh/g at 120 °C, 10% higher in capacity while operating at 30 °C lower. It is worth noting that the theoretical capacity, 531.6 mAh/g (Table 1S) is calculated by assuming the final discharge state is $Na_2S_2$. Nevertheless, the high performance clearly demonstrates that improving wetting of Na on the surface of BASE can dramatically lower cell interfacial resistance and

 

enhance cell capacity. We have observed a similar trend in performance at a higher current density of 2.33 mA/cm$^2$ (~C/7, Figure 1b, c, and d) with respect to different LAT treatment temperatures. At 120 °C, the LAT-550 cell shows the highest capacity of 438.3 mAh/g (2.33 mA/cm$^2$, ~C/7, Figure 1d). At current densities of 2.33, 4.67, 7, and 9.33 mA/cm$^2$, the LAT-550 cell has a capacity of 438.3, 310.3, 180.3, and 35.7 mAh/g, respectively. Comparing to BASE treated at lower temperatures, the LAT-550 cell shows the best performance at different rates (Figure 1e). For example, at a current density of 7 mA/cm$^2$, the cell capacity is 180.3 mAh/g, significantly higher than 117.3 mAh/g at 450 °C and 142.5 mAh/g at 500 °C.

Moreover, the LAT-550 cell shows improved long-term cyclability, with negligible degradation in cell capacity for over 1000 cycles when cycled at ~C/3.5 (Figure 1f). The specific capacity and energy density of the cell are 338.5 mAh/g (Figure 1f) and 596.1 Wh/kg (Figure 1S), respectively. In contrast, the LAT-450 cell loses about 25% of capacity in ~70 cycles (Figure 1b), and the LAT-500 cell (Figure 1c) shows a lower capacity than that of the LAT-550 cell with a slight degradation. In the current system, we attribute long-term stability to the wettability of Na on the BASE surface, as insufficient contact between the BASE and the Na anode can effectively limit the active area. The reduced active area further localizes current on spots of the BASE surface even though the nominal current density was low, which can eventually cause deterioration in performance during long-term cycling. On the contrary, the excellent wetting of the LAT-550 cell enables full and intimate contact between the BASE and the molten Na anode, which then distributes current evenly on the entire active area and thus stabilizes the battery components.

In our previous works, we have attributed the increase in performance and stability to greater sodium wettability, which were validated in our observation.[14] The wetting behavior of Na on BASE surfaces treated with LAT at 550 °C (Figure 2a) improves dramatically compared to that at 450 °C (Figure 2b and 2c). After 30 minutes, liquid Na starts a limited spreading to the neighboring area on the BASE treated with LAT at 450 °C. In contrast, liquid Na spreads over an area covered with LAT treated at 550 °C, and a full wetting is achieved with a wetting angle of ~0° within 5 minutes. Based on these observations, the higher LAT treatment temperature (e.g., 550 °C) is critical for Na to achieve agreeable wetting on BASE. A fully wetted BASE surface with Na is achieved at as low as 120 °C, which has never been reported in the literature to the best of our knowledge.

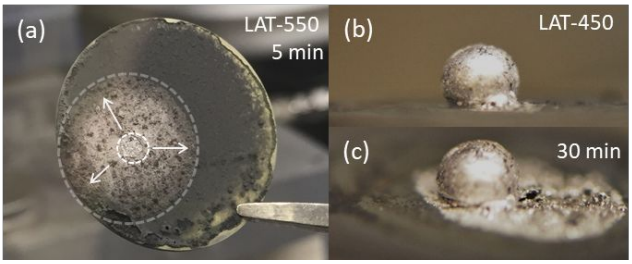


Figure 2. Wetting behavior of liquid Na droplets at 120 °C on BASE treated with LAT at 550 °C (a) and 450 °C (b and c). After 5 minutes, the BASE treated at 550 °C shows complete spreading (top view, a). The arrows indicate the spread from the original location. After 30 minutes, the BASE treated at 450 °C shows limited spreading (c).

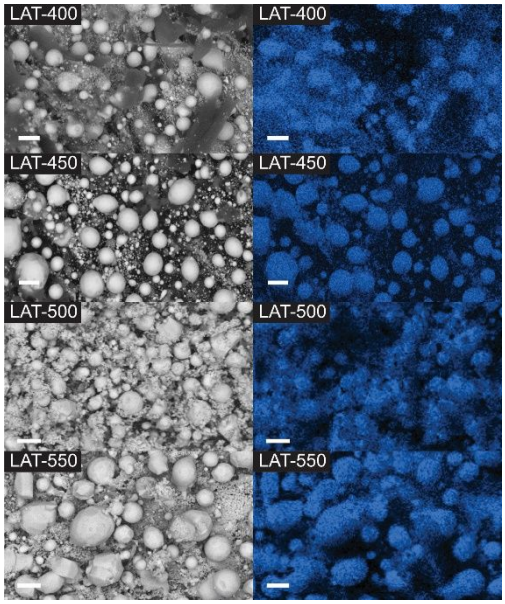


Figure 3. On the left, SEM images of the BASE surfaces treated at 400, 450, 500, and 550 °C. The corresponding Pb EDX maps on the right confirm the composition of spherical particles as Pb. All scale bars correspond to 2 μm.

To understand the mechanism behind the superior Na wettability, the microstructures of the BASE treated with LAT at 450, 500, and 550 °C are examined by scanning electron microscopy (SEM) and compared with a sample treated at 400 °C (Figures 3 and 2S). Overall, the morphologies are very similar, as micron-size Pb spherical particles coat the surface of BASE. Although slightly larger Pb particles with more well-defined faceting can form at higher treatment temperatures, the tremendous variation in wetting behavior unlikely stems from the differences in morphology alone (e.g., particle size and distribution).

Again, we turned to high-resolution XPS to elucidate the chemical composition of the surface layers on samples treated at 400 and 550 °C respectively (Figure 4a and 4b). We used a sputtering process to gradually remove the surface layer and expose the composition underneath. Each sputtering cycle can remove about a 2.5-nm-thick layer, which corresponds to about 15-nm-thick material after six cycles (see supplemental information). From the depth profile shown in Figure 4, the compositions of surface layers are initially similar for both samples. XPS bands at 138.2 and 143.4 eV match well with $Pb^{2+}$ species, and the metallic Pb bands are mostly absent from the surfaces.[19] As the sputtering progresses, metallic Pb phase ($Pb^0$ peaks at 142 and 136.8 eV) emerges after the second cycle (Figure 4a) in the sample treated at 400 °C. After six sputtering cycles, the peaks correlated to $Pb^{2+}$ species are still strong, indicating a significant presence of $Pb^{2+}$ compounds 15 nm from the surface. In comparison, Pb metallic phase appears immediately after the first cycle in the sample treated at 550 °C. After six sputtering cycles, metallic Pb is the dominant species instead. The ratios between two phases are quantified via peak fitting, and the relative contents of $Pb^{2+}$ compounds are plotted as a function of the sputtering depth from the surface (Figure 4c). Considering the native oxide layer (PbO) on metallic Pb only about 3—6 nm thick[20] and conversion to carbonate ($PbCO_3$)

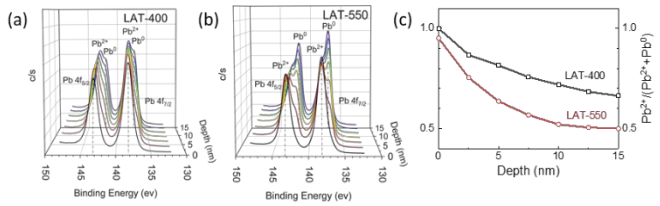


Figure 4. High-resolution XPS depth profiles of Pb element on BASE from LAT-400 (a) and LAT-550 (b) . The ratio of $Pb^{2+}$ and $Pb^{0}$ species (c) is calculated from the peak intensities of each species.

likely trapped during the growth of metallic particles from molten lead rather than converted from surface metallic Pb afterwards in a corrosion process. As we previously observed alloyed Na-Pb via $^{23}Na$ MAS NMR, physical contacts between sodium and lead were crucial for good Na wetting.[14] Instead, as these $Pb^{2+}$ species meet molten Na, metallic Pb and passivating ionic sodium byproducts form. Thus, the presence $Pb^{2+}$ species would create a low conduction pocket with passivating sodium salt and shift the alloying equilibrium. At higher temperatures, trapped $Pb^{2+}$ species can decompose more easily, and metallic Pb can form more uniform domains, both reducing passivation of the metallic Pb and resulting in better wettability.

In summary, we have demonstrated the performance of low-temperature (120 °C) Na-S battery is closely relating to the surface treatment of BASE with LAT at different temperatures. The drastic improvement in cell performances, both capacity and stability, supports our hypothesis that higher treatment temperatures would enhance the conversion to metallic lead by further activating the decomposition pathway of LAT and lowering oxidized surface contents. As we were examining the possible mechanisms, sodium wetting on solid electrolytes again presented itself as one of the central factors in cell performance. Innovations in surface modification reported in this work boost the interfacial activity of BASE even further at lower operating temperature (120 °C) and make sodium-based batteries more competitive in the upcoming challenges in large-scale energy storage.

## Conflicts of interest

There are no conflicts to declare.

## Notes and references

This work is mainly supported by the U.S. Department of Energy (DOE) Office of Electricity (OE) under contract DE-AC06-76LO1830 through Pacific Northwest National Laboratory (Cost competitive battery technology, project #70247) and the International Collaborative Energy Technology R&D Program of the Korea Institute of Energy Technology Evaluation and Planning (KETEP), the Ministry of Trade, Industry and Energy of the Republic of Korea (No. 20198510050010). X. Lu acknowledge the support from North Carolina A&T State University through a faculty start-up fund. Pacific Northwest National Laboratory is operated by Battelle for the DOE under Contract DE-AC05-76RL01830.

1. Z. G. Yang, J. L. Zhang, M. C. W. Kintner-Meyer, X. C. Lu, D. W. Choi, J. P. Lemmon and J. Liu, *Chem. Rev.*, 2011, **111**, 3577-3613.; B. Dunn, H. Kamath and J. M. Tarascon, *Science*, 2011, **334**, 928-935.
2. B. Diouf and R. Pode, *Renew. Energy*, 2015, **76**, 375-380.; B. H. Liu, Y. K. Jia, C. H. Yuan, L. B. Wang, X. Gao, S. Yin and J. Xu, *Energy Stor. Mater.*, 2020, **24**, 85-112.
3. B. L. Ellis and L. F. Nazar, *Curr. Opin. Solid State Mater. Sci.*, 2012, **16**, 168-177.
4. X. C. Lu, J. P. Lemmon, V. Sprenkle and Z. G. Yang, *JOM*, 2010, **62**, 31-36.
5. K. B. Hueso, M. Armand and T. Rojo, *Energy Environ. Sci.*, 2013, **6**, 734-749.
6. J. L. Sudworth, *J. Power Sources*, 2001, **100**, 149-163.
7. J. L. Sudworth and A. R. Tilley, *The Sodium Sulfur Battery*, Kluwer, New York, 1985.
8. Z. Y. Wen, J. D. Cao, Z. H. Gu, X. H. Xu, F. L. Zhang and Z. X. Lin, *Solid State Ionics*, 2008, **179**, 1697-1701.; T. Oshima, M. Kajita and A. Okuno, *Int. J. Appl. Ceram. Tec.*, 2004, **1**, 269-276.
9. Sodium-sulfur battery, https://en.wikipedia.org/wiki/Sodium-sulfur_battery, (accessed October 18, 2020).
10. J. K. Min, M. Stackpool, C. H. Shin and C. H. Lee, *J. Power Sources*, 2015, **293**, 835-845.
11. H. J. Chang, X. C. Lu, J. F. Bonnett, N. L. Canfield, S. Son, Y. C. Park, K. Jung, V. L. Sprenkle and G. S. Li, *J. Power Sources*, 2017, **348**, 150-157.
12. K. B. Hueso, V. Palomares, M. Armand and T. Rojo, *Nano Res.*, 2017, **10**, 4082-4114.
13. X. C. Lu, B. W. Kirby, W. Xu, G. S. Li, J. Y. Kim, J. P. Lemmon, V. L. Sprenkle and Z. G. Yang, *Energy Environ. Sci.*, 2013, **6**, 299-306.
14. H. J. Chang, X. C. Lu, J. F. Bonnett, N. L. Canfield, K. Han, M. H. Engelhard, K. Jung, V. L. Sprenkle and G. S. Li, *J. Mater. Chem. A*, 2018, **6**, 19703-19711.
15. D. Reed, G. Coffey, E. Mast, N. Canfield, J. Mansurov, X. C. Lu and V. Sprenkle, *J. Power Sources*, 2013, **227**, 94-100.
16. Y. Y. Hu, Z. Y. Wen, X. W. Wu and J. Jin, *J. Power Sources*, 2012, **219**, 1-8. ; Y. Y. Hu, Z. Y. Wen, X. W. Wu and Y. Lu, *J. Power Sources*, 2013, **240**, 786-795.; D. Jin, S. Choi, W. Jang, A. Soon, J. Kim, H. Moon, W. Lee, Y. Lee, S. Son, Y. C. Park, H. Chang, G. S. Li, K. Jung and W. Shim, *ACS Appl. Mater. Interfaces.*, 2019, **11**, 2917-2924.; G. S. Li, X. C. Lu, J. Y. Kim, J. P. Lemmon and V. L. Sprenkle, *J. Power Sources*, 2014, **249**, 414-417.; K. Ahlbrecht, C. Bucharsky, M. Holzapfel, J. Tubke and M. J. Hoffmann, *Ionics*, 2017, **23**, 1319-1327.; M. M. Gross, L. J. Small, A. S. Peretti, S. J. Percival, M. A. Rodriguez and E. D. Spoerke, *J. Mater. Chem. A*, 2020, **8**, 17012-17018.
17. X. C. Lu, G. S. Li, J. Y. Kim, D. H. Mei, J. P. Lemmon, V. L. Sprenkle and J. Liu, *Nat. Commun.*, 2014, **5**, 5578.
18. L. Y. Zhang, X. H. Xia, Y. Zhong, D. Xie, S. F. Liu, X. L. Wang and J. P. Tu, *Adv. Mater.*, 2018, **30**, 201804011.
19. K. S. Kim, T. J. Oleary and N. Winograd, *Anal. Chem.*, 1973, **45**, 2214-2218.; A. V. Naumkin, A. Karunt-Vass, S. W. Gaarenstroom and C. J. Powell, NIST X-ray Photoelectron Spectroscopy Database, *https://srdata.nist.gov/xps/Default.aspx*, (accessed October 18, 2020).
20. C. Leygraf, I. O. Wallinder, J. Tidblad and T. Graedel, *Atomspheric Corrosion*, Wiley, 2016.
21. S. A. A. Sajadi and A. A. Alamolhoda, *Inorg. Mater.*, 2006, **42**, 1099-1103.; Y. J. Xie, Y. Wang, V. Singhal and D. E. Giammar, *Environ. Sci. Technol.*, 2010, **44**, 1093-1099.

## TOC Graphics

$Pb(OAc)_2 \cdot 3H_2O$ (LAT)
> 400 °C, Up to 550 °C

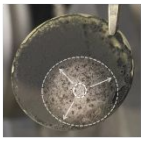

Surface-modified BASE
Complete Na wetting at 120 °C

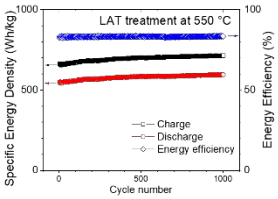


Improved battery capacity and stability